Int. J. Solids Structures, 1969, Vol. 5, pp. 437 to 454. Pergamon Press. Printed in Great Britain

SHADOW-ZONE RESPONSE IN THE DIFFRACTION OF A PLANE COMPRESSIONAL PULSE BY A CIRCULAR CAVITY*

J. C. PECK

Staff Engineer, McDonnell Douglas Astronautics Company, Western Division, Santa Monica, California

and

J. MIKLOWITZ

Professor of Applied Mechanics, California Institute of Technology, Pasadena, California

Abstract—This paper discusses the two-dimensional interaction of a step-function compressional wave with a circular cavity in an infinite elastic medium. The technique presented here is an adaptation of a method developed by Friedlander for wave-front approximations. Friedlander's method proves more accurate for short times than the Fourier series approach. The presented work exploits, for the first time, the application of a numerical technique to Friedlander's basic method. The numerical technique is applicable only in the shadow zone of the cavity, which is the only region where the solution can be constructed from the transient response in a series of circumferential propagation modes. These modes are governed by a dispersive spectrum relating complex wave numbers to frequency. Numerical results are presented for seven modes of the spectrum. These modes are used to construct the transient velocities on the back surface of the cavity. The numerical results indicate that the convergence of the mode series is very rapid at short times, and that seven modes are sufficient to determine the long-time asymptotic values. Comparisons of the present results with earlier Fourier series results show the latter's degree of inaccuracy at short time.

INTRODUCTION

IN RECENT years there have been many analyses of the two-dimensional (plane strain) interaction of transient elastic waves with a circular cylindrical obstacle in an otherwise unbounded medium. These analyses are primarily motivated by the relationship of the interaction problem to the effects of ground shock waves on underground structures [1]. Most of these studies use a Fourier series representation of dependence of the solution on the circumferential coordinate, θ. Recently, a new technique was developed by Friedlander [2, 3], essentially using a Fourier integral representation of the θ dependence and representing the solution in terms of circumferentially propagating waves. The latter representation will be referred to in this paper as the "wave-sum" type of solution.

The Fourier series representation is an effective means of solution at long times and/or large distances from the obstacle. Through use of numerical techniques and electronic digital computers, however, the Fourier series solutions have been evaluated for points near the obstacle surface at times as short as one transit time, i.e. the time required for an incident wave to pass across the obstacle [4–7].

Previous to the work described herein, the Friedlander wave-sum type of solution was used only for approximate evaluations, valid close to wave arrival times. Gilbert and Knopoff [8] and Gilbert [9] used this method to obtain wave-front approximations for

* Presented to the Fifth U.S. National Congress of Applied Mechanics, University of Minnesota, Minneapolis, Minnesota, 14–17 June 1966.

the dilatation (P) and shear (S) wave fronts generated by impulsive line sources. Miklowitz [10, 11] supplemented the Friedlander technique with a contour-integration treatment and obtained an approximation for the Rayleigh-type wave (caused by an incident plane dilatation wave) on the surface of a cavity. Grimes [12] obtained P and S wave-front approximations in the illuminated zone for the case of an incident plane wave. Norwood and Miklowitz [13] recently obtained approximations for the diffracted P and Rayleigh waves for the case of a spherical cavity.

The work presented here is a numerical evaluation of the wave-sum solution for the case of a plane, step-function stress, dilatation wave incident upon a cavity (Fig. 1). This is

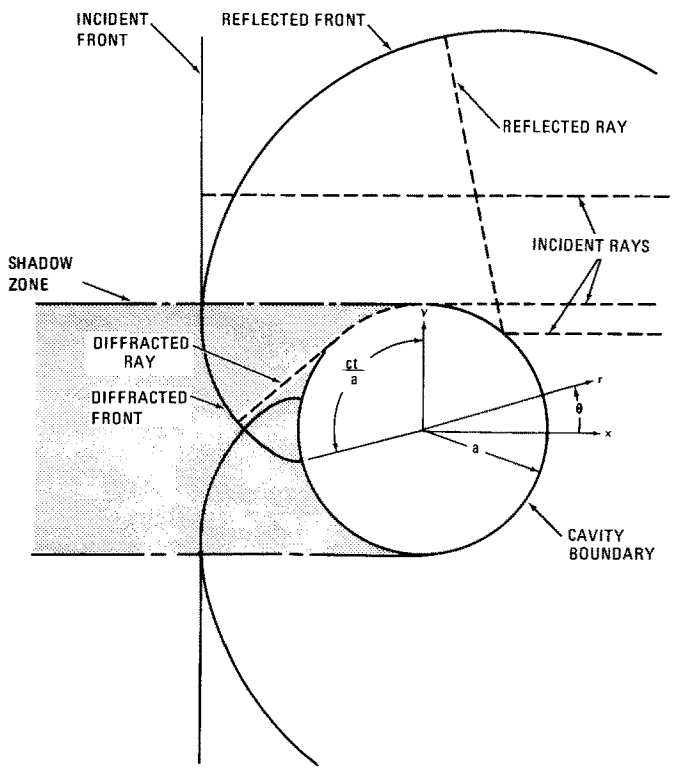

FIG. 1. Geometry of the problem, showing the dilatational wave fronts at a time after the incident front has passed the cavity.

apparently the first time the wave-sum method has been exploited numerically. The technique is particularly effective for short times, as expected. In addition, the convergence properties of the solution are good even for rather long times, say five transit times.

An important concept related to the method used here is the division of space into the so-called shadow and illuminated zones. The shadow zone consists of those points that can be reached from the source only by diffracted rays, i.e. minimum time paths that lie, in part, on the surface of the cavity. The remaining portion of space is the illuminated zone (see [9] for a more detailed discussion). Plane waves may be regarded as originating from a source at infinity, therefore the shadow zone for the subject problem is as shown in Fig. 1.

The numerical results presented here were obtained only in the shadow zone. In this region, one of the two inversion integrals involved in Friedlander's technique can be expressed as an infinite series of residues. Each term of the series corresponds to a mode of circumferential wave propagation. These modes are similar to those found in rod and plate theory. The transient response is found by numerical evaluation of the second inversion integral for each term of the mode series. There is no apparent way to apply direct numerical evaluation of Friedlander-type solutions in the illuminated zone. The residue evaluation in this region is inappropriate; therefore both inversion integrals would have to be evaluated numerically. Direct numerical evaluation of both inversion integrals would be difficult, if not impossible.

Even in the shadow-zone evaluations, the numerical work is formidable and must be backed up by various lengthy asymptotic approximations. Difficulties with slow convergence of the infinite integrals for the stresses still persist, therefore the results obtained were limited to the velocities and displacements.

INITIAL-BOUNDARY VALUE PROBLEM

The problem is formulated in terms of displacement potentials, ϕ and $\boldsymbol{\Psi}$. Let the vector displacement, $\mathbf{u}$, be given by $\mathbf{u} = \nabla\phi + \nabla \times \boldsymbol{\Psi}$. In this case, $\boldsymbol{\Psi}$ has only one nonzero component (denoted by ψ), perpendicular to the plane of the problem. Then one has the well-known result that solutions of the wave equations

$$\nabla^2\phi = \frac{\partial^2\phi}{\partial r^2} + \frac{1}{r}\frac{\partial\phi}{\partial r} + \frac{1}{r^2}\frac{\partial^2\phi}{\partial\theta^2} = \frac{1}{c_d^2}\frac{\partial^2\phi}{\partial t^2}, \qquad c_d^2 \equiv \frac{\lambda+2\mu}{\rho} \tag{1a}$$

$$\nabla^2\psi = \frac{\partial^2\psi}{\partial r^2} + \frac{1}{r}\frac{\partial\psi}{\partial r} + \frac{1}{r^2}\frac{\partial^2\psi}{\partial\theta^2} = \frac{1}{c_s^2}\frac{\partial^2\psi}{\partial t^2}, \qquad c_s^2 \equiv \frac{\mu}{\rho} \tag{1b}$$

are also solutions of the displacement equation of motion for a linear, elastic, isotropic, homogeneous solid. λ and μ are the Lamé constants and ρ is the density. The radial and circumferential displacement components, denoted by u and v, respectively, and the stresses σ_r, σ_θ, and $\tau_{r\theta}$ are related to the potentials by

$$u = \frac{\partial\phi}{\partial r} + \frac{1}{r}\frac{\partial\psi}{\partial\theta} \tag{2a}$$

$$v = \frac{1}{r}\frac{\partial\phi}{\partial\theta} - \frac{\partial\psi}{\partial r} \tag{2b}$$

$$\sigma_r = (\lambda+2\mu)\nabla^2\phi + 2\mu\left(-\frac{1}{r}\frac{\partial\phi}{\partial r} - \frac{1}{r^2}\frac{\partial^2\phi}{\partial\theta^2} - \frac{1}{r^2}\frac{\partial\psi}{\partial\theta} + \frac{1}{r}\frac{\partial^2\psi}{\partial r\partial\theta}\right) \tag{3a}$$

$$\sigma_\theta = (\lambda+2\mu)\nabla^2\phi - 2\mu\left(\frac{\partial^2\phi}{\partial r^2} - \frac{1}{r^2}\frac{\partial\psi}{\partial\theta} + \frac{1}{r}\frac{\partial^2\psi}{\partial r\partial\theta}\right) \tag{3b}$$

$$\tau_{r\theta} = \mu\left(\frac{2}{r}\frac{\partial^2\phi}{\partial r\partial\theta} - \frac{2}{r^2}\frac{\partial\phi}{\partial\theta} + \frac{1}{r^2}\frac{\partial^2\psi}{\partial\theta^2} - \frac{\partial^2\psi}{\partial r^2} + \frac{1}{r}\frac{\partial\psi}{\partial r}\right). \tag{3c}$$

The solution is separated into scattered and incident parts, denoted by subscripts $(\ )_{sc}$ and $(\ )_{inc}$, respectively. The total solution is given by the sum of the scattered and incident parts, e.g. $\phi = \phi_{sc} + \phi_{inc}$. Each part satisfies the wave equations. The incident part is

specified to be a step–stress dilatation wave,

$$\phi_{\text{inc}} = \frac{\sigma_0 c_d^2}{\lambda+2\mu}\left(t+\frac{r\cos\theta}{c_d}\right)^2 H\left(t+\frac{r\cos\theta}{c_d}\right). \tag{4}$$

Then the incident stresses are also known, and the boundary conditions for the scattered solution are

$$\sigma_{r_{\text{sc}}}(a,\theta,t) = -\sigma_{r_{\text{inc}}}(a,\theta,t) \tag{5a}$$

$$\tau_{r\theta_{\text{sc}}}(a,\theta,t) = -\tau_{r\theta_{\text{inc}}}(a,\theta,t) \tag{5b}$$

at $r = a$, in order that the total stress on the surface of the cavity be zero. Inasmuch as the incident wave first strikes the cavity at $t = -a/c_d$, the mathematical specification of the problem for the scattered potentials is completed by requiring

$$\phi_{\text{sc}} = \frac{\partial\phi_{\text{sc}}}{\partial t} = \psi_{\text{sc}} = \frac{\partial\psi_{\text{sc}}}{\partial t} = 0$$

at $t = -a/c_d$.

GEOMETRY OF THE WAVE FRONTS

Because the method of solution is intimately connected with the wave-front propagation, a description of the fronts is presented at this point. Fig. 1 shows the positions of the incident, reflected, and diffracted dilatational wave fronts shortly after the incident front has passed the cavity.

The fronts may be regarded as propagating along rays. Rays that lie partly on a bounding surface are called diffracted rays. Points that can be connected to the source of disturbance only by diffracted rays are said to lie in the shadow zone. For the present problem, the source of the disturbance is at $r = \infty$, $\theta = 0$, hence the shadow zone for dilatational waves is as shown in Fig. 1. A larger shadow zone is associated with the shear waves [9], but it encompasses the dilatational shadow zone. For this reason, the only region completely in the shadow is the dilatational shadow zone.

The wave fronts may be constructed by using the fact that they propagate along the rays at the wave speeds c_d and c_s. The position of the diffracted dilatational front on $r = a$ is particularly simple, being merely

$$\theta = \frac{c_d t}{a}+\frac{\pi}{2},$$

since $t = 0$ is taken when the incident front passes the center of the cavity. Thus, an increase of 2π in $c_d t/a$ returns the front on $r = a$ to the same position. This "winding" of the diffracted front continues *ad infinitum*.

FRIEDLANDER'S REPRESENTATION OF THE SOLUTION

The method of solution suitable for short-time evaluations was developed by Friedlander [2, 3]. This form may be obtained by various means. Perhaps the most direct

method is the application of Poisson's summation formula [14], which may be stated

$$\sum_{n=-\infty}^{\infty} g(n) = \sum_{m=-\infty}^{\infty} \int_{-\infty}^{\infty} g(\xi) e^{2m\pi\xi i}\, d\xi.$$

Applied to the Fourier series representation of a typical response function $f(r, \theta, t)$, this gives

$$\begin{aligned} f(r, \theta, t) &= \sum_{n=-\infty}^{\infty} F(r, n, t) e^{in\theta} \\ &= \sum_{m=-\infty}^{\infty} \int_{-\infty}^{\infty} F(r, \xi, t) e^{i\xi(\theta + 2m\pi)}\, d\xi \\ &= \sum_{m=-\infty}^{\infty} f^*(r, \theta + 2m\pi, t) \end{aligned} \tag{6}$$

where the definition

$$f^*(r, \theta, t) \equiv \int_{-\infty}^{\infty} F(r, \xi, t) e^{i\xi\theta}\, d\xi \tag{7}$$

is used in equation (6). For reasons that will become clear later, f^* is called the "wave form" of f, and the sum on m in equation (6) is called the "wave sum".

The wave form of the response, f^*, has a clear physical interpretation. This response is the disturbance propagating outward in θ with the wave fronts given by the geometrical theory above, i.e. the fronts of f^* wind around the cavity. From his wave-front expansions, Friedlander found that f^* is identically zero for θ's beyond the wave front, therefore, for finite t, the sum on m is finite. Thus, f^* overlaps itself as it winds around the cavity, and the wave sum on m is simply the sum of the overlapping responses. Both the total solution f and the wave form f^* are defined on $-\infty < \theta < \infty$, but f^* is not periodic in θ; however, the wave sum on m gives the total solution the 2π periodicity in θ that is physically required. This may be seen by asking for the value of f at a θ that is outside the usual physical range, say $\theta = 4\pi$ instead of $\theta = 0$. All this means is that in equation (6) the terms that contribute to the total solution differ (from the solution for $\theta = 0$) by 2 in their value of m, but the number of terms and the values of the individual terms are identical to the $\theta = 0$ case. See [3] for additional discussion of the interpretation of the solution.

The present problem can be cast in the wave-sum form by first finding the Fourier series representation of the solution, and then applying the above formulas; however, a more direct method is as follows. Because the only given function in the problem is the incident potential, once its expression in the wave-sum form is found, one can simply require that each term of the wave sum for ϕ_{sc} and ψ_{sc} satisfy the wave equations,

$$\frac{\partial^2 \phi_{sc}^*}{\partial r^2} + \frac{1}{r}\frac{\partial \phi_{sc}^*}{\partial r} + \frac{1}{r^2}\frac{\partial^2 \phi_{sc}^*}{\partial \theta^2} = \frac{1}{c_d^2}\frac{\partial^2 \phi_{sc}^*}{\partial t^2} \tag{8a}$$

$$\frac{\partial^2 \psi_{sc}^*}{\partial r^2} + \frac{1}{r}\frac{\partial \psi_{sc}^*}{\partial r} + \frac{1}{r^2}\frac{\partial^2 \psi_{sc}^*}{\partial \theta^2} = \frac{1}{c_s^2}\frac{\partial^2 \psi_{sc}^*}{\partial t^2} \tag{8b}$$

and that the boundary conditions are also satisfied term-by-term

$$\sigma^*_{r_{sc}}(a, \theta, t) = -\sigma^*_{r_{inc}}(a, \theta, t) \tag{9a}$$

$$\tau^*_{r\theta_{sc}}(a, \theta, t) = -\tau^*_{r\theta_{inc}}(a, \theta, t). \tag{9b}$$

When the quiescent initial conditions at $t = -a/c_d$ are added, it is clear that the wave sum of the solutions to the above problem is the solution to the original problem. To complete the statement of the problem, the wave-sum form of the incident potential must be obtained. This is done after the application of integral transforms.

TRANSFORM SOLUTION

The bilateral Laplace transform on time will be denoted by

$$\bar{f}(r, \theta, p) = \int_{-\infty}^{\infty} f(r, \theta, t)e^{-pt}\,dt \tag{10a}$$

with the inversion integral

$$f(r, \theta, t) = \frac{1}{2\pi i}\int_{Br_1} \bar{f}(r, \theta, p)e^{pt}\,dp. \tag{10b}$$

Br_1 is the Bromwich contour, $\mathscr{R}p = c$, $-\infty < \mathscr{I}p < \infty$. The subsequent Fourier transform on θ is denoted by

$$\tilde{f}(r, \nu, p) = \int_{-\infty}^{\infty} \bar{f}(r, \theta, p)e^{-i\nu\theta}\,d\theta \tag{11a}$$

with the inversion integral

$$\bar{f}(r, \theta, p) = \frac{1}{2\pi}\int_{-\infty}^{\infty} \tilde{f}(r, \nu, p)e^{i\nu\theta}\,d\nu. \tag{11b}$$

The double transform of the wave-sum form of the incident potential is found by applying the Poisson summation formula to the Fourier series of the Laplace transform of ϕ_{inc}. From equation (4), $\bar{\phi}_{inc} = \bar{\phi}_0(p)\exp(k_d r\cos\theta)$, where $k_d = p/c_d$ and $\bar{\phi}_0(p) = \sigma_0 c_d^2 p^{-3}(\lambda+2\mu)^{-1}$. The Fourier series may be written as

$$\bar{\phi}_{inc}(r, \theta, p) = \sum_{n=-\infty}^{\infty} \bar{\phi}_0(p)I_{|n|}(k_d r)e^{in\theta}$$

where the integral definition of I_n, the modified Bessel function of the first kind, has been used. The absolute value sign is permissible since $I_{-n}(z) = I_n(z)$ for integral n. Then, applying equation (7) and taking the Fourier transform gives

$$\tilde{\phi}^*_{inc}(r, \nu, p) = \phi_0(p)\int_{-\infty}^{\infty}\int_{-\infty}^{\infty} I_{|\xi|}(k_d r)e^{i\theta(\xi-\nu)}\,d\xi\,d\theta.$$

Since $I_\nu(z)$ approaches zero exponentially as $\nu \to +\infty$, the Fourier integral theorem gives

$$\tilde{\phi}^*_{inc}(r, \nu, p) = 2\pi\bar{\phi}_0(p)I_{|\nu|}(k_d r). \tag{12}$$

Applying the Laplace–Fourier transform to equations (8) for ϕ^*_{sc} and ψ^*_{sc} gives the equations for the modified Bessel functions. Using only those solutions that vanish as $r \to \infty$, one obtains

$$\tilde{\phi}^*_{sc}(r, \nu, p) = A(\nu, p)K_\nu(k_d r) \tag{13a}$$

$$\tilde{\psi}^*_{sc}(r, \nu, p) = B(\nu, p)K_\nu(k_s r) \tag{13b}$$

where $k_s = p/c_s$ and K_ν is the modified Bessel function of the second kind. A and B are determined from the boundary conditions at $r = a$. Applying the transformed stress expressions

$$\tilde{\sigma}^*_r = \mu r^{-2}\left[(k_s^2 r^2 + 2\nu^2)\tilde{\phi}^* - 2r\frac{d\tilde{\phi}^*}{dr} - 2i\nu\left(\tilde{\psi}^* - r\frac{d\tilde{\psi}^*}{dr}\right)\right] \tag{14a}$$

$$\tilde{\tau}^*_{r\theta} = \mu r^{-2}\left[-2i\nu\left(\tilde{\phi}^* - r\frac{d\tilde{\phi}^*}{dr}\right) - (2\nu^2 + k_s^2 r^2)\tilde{\psi}^* + 2r\frac{d\tilde{\psi}^*}{dr}\right] \tag{14b}$$

to the transformed boundary conditions gives

$$\begin{aligned} A(\nu, p) = {} & [D(\nu, p)]^{-1} 2\pi\bar{\phi}_0(p)\{[(2\nu^2 + k_s^2 a^2)I_{|\nu|}(k_d a) - 2k_d a I'_{|\nu|}(k_d a)] \\ & \times [(2\nu^2 + k_s^2 a^2)K_\nu(k_s a) - 2k_s a K'_\nu(k_s a)] \\ & - 4\nu^2[I_{|\nu|}(k_d a) - k_d a I'_{|\nu|}(k_d a)] \cdot [K_\nu(k_s a) - k_s a K'_\nu(k_s a)]\} \end{aligned} \tag{15}$$

$$B(\nu, p) = -[D(\nu, p)]^{-1} 4\pi\bar{\phi}_0(p) i\nu(2\nu^2 + k_s^2 a^2 - 2) \tag{16}$$

where

$$\begin{aligned} D(\nu, p) = {} & -\{[(2\nu^2 + k_s^2 a^2)K_\nu(k_d a) - 2k_d a K'_\nu(k_d a)] \cdot [(2\nu^2 + k_s^2 a^2)K_\nu(k_s a) - 2k_s a K'_\nu(k_s a)] \\ & - 4\nu^2[K_\nu(k_d a) - k_d a K'_\nu(k_d a)] \cdot [K_\nu(k_s a) - k_s a K'_\nu(k_s a)]\}. \end{aligned} \tag{17}$$

The Wronskian $K_\nu(z)I'_\nu(z) - K'_\nu(z)I_\nu(z) = z^{-1}$ has been used to simplify the expression for B. The expressions for the transformed scattered displacements and circumferential stress are

$$\tilde{u}^*_{sc}(r, \nu, p) = r^{-1}[k_d r K'_\nu(k_d r)A(\nu, p) + i\nu K_\nu(k_s r)B(\nu, p)] \tag{18a}$$

$$\tilde{v}^*_{sc}(r, \nu, p) = r^{-1}[i\nu K_\nu(k_d r)A(\nu, p) - k_s r K'_\nu(k_s r)B(\nu, p)] \tag{18b}$$

$$\begin{aligned} \tilde{\sigma}^*_{\theta sc}(r, \nu, p) = {} & \mu r^{-2}\{[(k_s^2 r^2 - 2\nu^2 - k_d^2 r^2)K_\nu(k_d r) + 2k_d r K'_\nu(k_d r)]A(\nu, p) \\ & - 2i\nu[K_\nu(k_s r) - k_s r K'_\nu(k_s r)]B(\nu, p)\}. \end{aligned} \tag{18c}$$

INVERSION OF THE TRANSFORMED SOLUTION

The Fourier transform will be inverted by contour integration in the complex ν plane, therefore the analyticity of the transforms in ν must be examined. First, the absolute value signs on ν may be dropped when the sum of the scattered and incident response is considered, since $\phi^*_{sc} + \phi^*_{inc}$ is even in real ν, regardless of whether or not the absolute value signs are used. Then the continuation off the real ν axis is immediate, because the Bessel functions are entire when considered as a function of their order as a complex variable. The only possible singularities in ν of the transforms arise from zeros of the denominator $D(\nu, p)$.

It will be seen below that D has an infinity of simple complex zeros, $v_j(p)$, which approach infinity as $j \to \infty$.

The Fourier inversion integral is then evaluated using the residue theorem. The inversion contour on the real axis is completed by a sequence of curves C_j passing between the zeros v_j. Provided that $|\theta| > \pi/2$ and that C_j is taken in $\mathscr{I}v \gtrless 0$ for $\theta \lessgtr 0$, the integrals on C_j vanish as $j \to \infty$ and the integral on real v is equal to the convergent infinite series of the residues at v_j. The usefulness of the series in computations is, however, restricted to the shadow zone where the series is rapidly convergent. No proof of these restrictions is offered here, but they are characteristic of the wave-sum approach to the problem. Detailed discussions of such restrictions for similar problems may be found in references [3], [13] and [15].

For the sake of brevity, in the remainder of this paper let f denote any of the response functions, such as u, v, σ_θ, etc. Then the residue evaluation yields

$$\bar{f}^*(r, \theta, p) = \sum_j \bar{f}_j^*(r, \theta, p) \tag{19}$$

where

$$\bar{f}_j^*(r, \theta, p) = -i\{\bar{f}_{sc}^*(r, v, p)e^{iv\theta}D(v, p)[\partial D/\partial v]^{-1}\}_{v=v_j}. \tag{20}$$

For the numerical computations, it is worthwhile to note that

$$[\partial D/\partial v]_{v=v_j} = -[(\partial D/\partial p)(dv/dp)^{-1}]_{v=v_j}$$

since $D(v_j, p) = 0$.

The Laplace transform inversion of $\bar{f}^*$ must now be found. It is reasonable to assume that f^* does not grow exponentially in time, in which case $\bar{f}^*$ must be analytic in $\mathscr{R}p > 0$, and Br_1 may be chosen with $\mathscr{R}p = c$ for any $c > 0$. The Br_1 contour is completed by the contour $C + C_R + C_{-R}$, as shown in Fig. 2. This contour is taken on the imaginary axis in order to give p the character of frequency, which allows greater physical insight, and also because it has been successfully used in other numerical evaluations [16, 17]. The indentation C_0 avoids the branch point $p = 0$ common to the Bessel functions. Assuming that the integrals on $C_{\pm R}$ vanish, and that the sum on j may be interchanged with the integral on C, one finds

$$f^*(r, \theta, t) = \sum_j f_j^*(r, \theta, t) \tag{21}$$

where

$$f_j^*(r, \theta, t) = f_{j_F}^*(r, \theta, t) + f_{j_0}^*(r, \theta, t) \tag{22a}$$

$$f_{j_F}^*(r, \theta, t) = \frac{1}{2\pi i} \lim_{\substack{R \to \infty \\ \delta \to 0}} \int_{-iR}^{-i\delta} + \int_{i\delta}^{iR} \bar{f}_j^*(r, \theta, p)e^{pt}\, dp \tag{22b}$$

and

$$f_{j_0}^*(r, \theta, t) = -\frac{1}{2\pi i} \lim_{\delta \to 0} \int_{C_0} \bar{f}_j^*(r, \theta, p)e^{pt}\, dp \tag{22c}$$

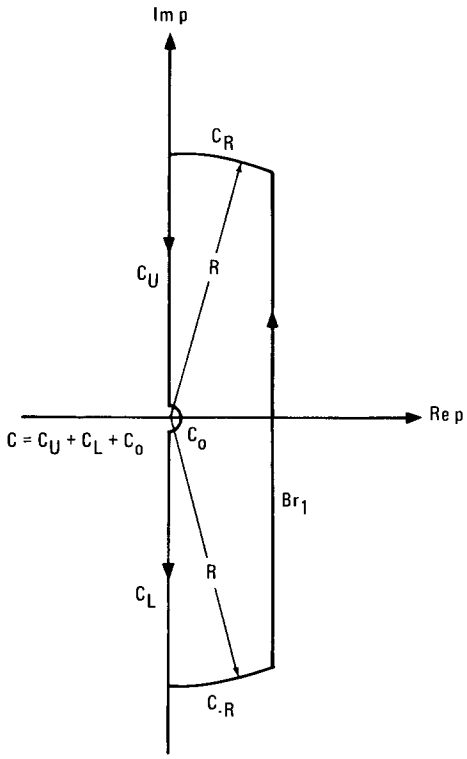

FIG. 2. Completion of inversion contour for Laplace transform.

in which the radius of C_0 is denoted by δ. For the integral $f^*_{j_F}$ on the imaginary axis, we may set $p = -i\omega$ where ω is real, and write

$$f^*_{j_F}(r, \theta, t) = \lim_{\substack{R\to\infty \\ \delta\to 0}} -\frac{1}{2\pi}\left[\int_{-R}^{-\delta} + \int_{\delta}^{R}\right] \{\tilde{f}^*_{sc}(r, v, -i\omega)D(v, -i\omega) \cdot [\partial D/\partial v]^{-1} e^{i(v\theta - \omega t)}\}_{v=v_j(-i\omega)} \, d\omega. \tag{23}$$

The form of the integrand in equation (23) brings out a very important point. Notice that the factor $e^{i(v_j\theta - \omega t)}$ represents a circumferentially propagating wave which is a pure sinusoid in time (with frequency ω), but a decaying sinusoid in θ. It decays in θ because (as will be seen below) the wave number, v_j, is complex with a positive imaginary part. The dependence of v_j on ω may be said to define a mode of sinusoidal wave propagation. Then one has the obvious and useful interpretation of the integral over ω as the transient response in such a mode. For this reason, we call the sum on j in equation (21) the "mode sum".

Before further evaluation of the integrals, it is necessary to delineate the nature of the $v_j - \omega$ relationship in detail.

BEHAVIOR OF THE ROOTS OF THE FREQUENCY EQUATION

The functions $v_j(-i\omega)$ are the roots of the equation $D(v, -i\omega) = 0$. This equation is called the frequency equation because it determines the relationship between the wave

number and frequency in sinusoidal wave propagation modes. Using the relationship $K_\nu(z\,e^{-i(\pi/2)}) = \frac{1}{2}i\pi\,e^{\frac{1}{2}\nu\pi i}H_\nu(z)$, one can write the frequency equation as

$$D(\nu, -i\omega) = \left(\frac{\pi}{2}\right)^2 e^{\nu\pi i}\{[(2\nu^2-\Omega_s^2)H_\nu(\Omega)-2\Omega H'_\nu(\Omega)]\,.\,[(2\nu^2-\Omega_s^2)H_\nu(\Omega_s)-2\Omega_s H'_\nu(\Omega_s)]$$
$$-4\nu^2[H_\nu(\Omega)-\Omega H'_\nu(\Omega)]\,.\,[H_\nu(\Omega_s)-\Omega_s H'_\nu(\Omega_s)]\} = 0 \tag{24}$$

where $\Omega = \omega a/c_d$, $\Omega_s = \omega a/c_s$, and $H_\nu(z)$ denotes the Hankel function of the first kind.† Using Bessel function recursion relations, one can also write this as

$$D(\nu, -i\omega) = \frac{1}{2}\Omega^2\Omega_s^2\left(\frac{\pi}{2}\right)^2 e^{\nu\pi i}\{H_{\nu+2}(\Omega)H_{\nu-2}(\Omega_s)+H_{\nu-2}(\Omega)H_{\nu+2}(\Omega_s)$$
$$-(\alpha^2-1)H_\nu(\Omega)[H_{\nu+2}(\Omega_s)+H_{\nu-2}(\Omega_s)]\} = 0 \tag{25}$$

where $\alpha = c_d/c_s$.

The frequency equation for the present problem was first obtained by Victorov [18] in the form given in equation (25). He found an approximation for a root whose velocity approached the Rayleigh velocity c_R as $\Omega \to +\infty$. Later, Gilbert [9] found approximations for an infinity of roots whose velocities approach c_d as $p \to \infty$ on the real p axis.

The similar but simpler frequency equations governing the analogous acoustic and electromagnetic problems have been studied extensively. The recent work of Keller *et al.* [19] presents a comprehensive summary of asymptotic and numerical results for these problems.

Here we present numerical results for the present problem for real Ω (imaginary p), but merely quote the corresponding asymptotic approximations for large and small Ω. The derivations of the approximations are too lengthy for inclusion here, however, they are given in [20]. The present large-Ω results are very similar to those of Nagase [21], who gives an extensive discussion of the large-Ω asymptotic behavior of the roots for the diffraction of sinusoidal elastic waves by a spherical cavity.

The roots have useful symmetry properties. The integral definition of $K_\nu(z)$ shows that $K_\nu(z) = K_{-\nu}(z)$ and $K_{\bar\nu}(\bar z) = \overline{K_\nu(z)}$ (in this paragraph bars are used to denote complex conjugates). Then an examination of equation (17) shows that $D(-\nu, p) = D(\nu, p)$ and $D(\bar\nu, \bar p) = \overline{D(\nu, p)}$. This means that if $\nu_0(p)$ is a root, $-\nu_0(p)$ and $\pm\bar\nu_0(\bar p)$ are also roots. Therefore all the roots for real Ω may be found from the roots with $\mathscr{I}\nu > 0$ and $\Omega > 0$.

Numerical results for seven of the roots are shown in Fig. 3 for real Ω and the $\mathscr{I}\nu > 0$ half of the complex ν plane. These and the later transient response results all use a Poisson's ratio of $\frac{1}{4}$. All other physical and geometrical constants are eliminated by nondimensionalization. These numerical results were obtained by using a FORTRAN computer program from the SHARE library [22] to calculate the Bessel functions of complex order, and a root-finder program based on the method of false position. The determination of each root at the points Ω = 0·01(0·01) 0·1(0·1) 1(0·2) 2(0·5) 5(1) 40‡ required about 5 minutes on an IBM 7094 computer.§ For reference purposes, note that a line, $\Omega = \mathscr{R}\nu$, would correspond to waves propagating at velocity c_d. The three roots designated $P1$, $P2$, and

† The superscript in the conventional notation $H_\nu^{(1)}$, is omitted for convenience. Hankel functions of the second type are not used in this paper.

‡ The notation $a(b)c$ means that increments of length b were used between values a and c.

§ About half of the computer time for the present work was provided gratis by the Western Data Processing Center at the University of California, Los Angeles, under their off-campus users' program.

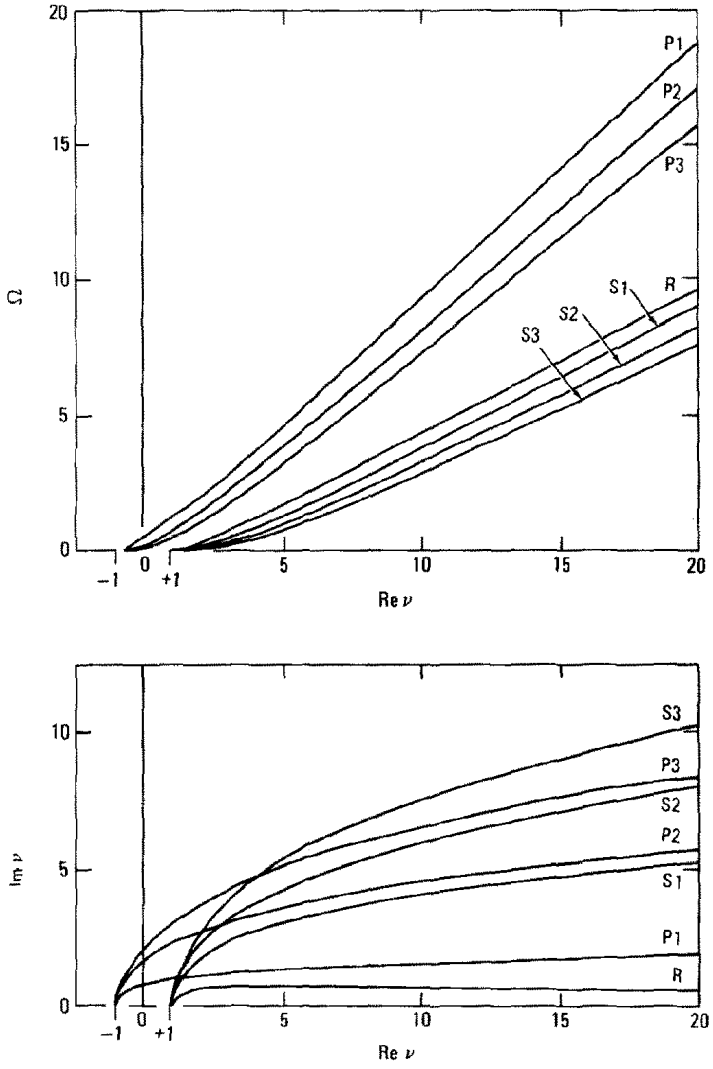

FIG. 3. Projections of the roots.

$P3$ are the first three of an infinity of roots whose phase velocities approach c_d as Ω approaches infinity. Their asymptotic approximation, to two terms, is

$$\nu_j \sim \Omega + a_j \left(\frac{\Omega}{2}\right)^{\frac{1}{3}} e^{-2/3\pi i} \tag{26}$$

where the a_j are the roots of the Airy function ($a_1 = -2.338\ldots$, etc.). The three roots designated $S1$, $S2$, and $S3$ are the first three of an infinity of roots whose phase velocities approach c_s and have approximations corresponding to equation (26) with Ω replaced

by Ω_s. The root designated R is a single root whose velocity approaches the Rayleigh velocity. The wave number of this root has the approximation

$$\nu_R \sim \frac{c_d}{c_R}\Omega + \gamma_1 + i\gamma_2\Omega e^{-\gamma_3\Omega} \tag{27}$$

where the γ_i are real positive functions of c_d and c_s. The expressions for the γ_i may be found in [20] or by reference to Victorov [18].

All the roots are complex; the lower half of Fig. 3 shows the behavior of $\mathscr{I}\nu$. As $\mathscr{R}\nu$ (and hence Ω) grows, $\mathscr{I}\nu$ also grows for the P and S roots. For the R root, $\mathscr{I}\nu$ first grows and then decreases to zero. Thus, according to equation (23), the R root should play the most important role for large θ.

As Ω approaches zero, the P roots approach $\nu = -1$, and the S roots and R root approach $\nu = +1$. The low-frequency approximation need be written only for $\nu \doteq +1$, because the $\nu \doteq -1$ behavior follows from symmetry:

$$\nu_j(p) = 1 - \frac{1}{2}\left[\log\frac{\alpha^2+1}{\alpha^2-1} + (2j+1)\pi i\right]\left(\log\frac{pa}{c_d}\right)^{-1} + O[(\log p)^{-2}] \tag{28}$$

where $j = 0$ corresponds to the R root, $j > 0$ to the S roots, and $j < 0$ to the P roots.

Using this information about the roots ν_j, the contour integral for the inverse Laplace transforms f_j^* given by equation (22) will now be evaluated on the surface of the cavity, $r = a$.

SINGULARITIES OF THE INTEGRANDS AT $p = 0$

Consider first the behavior of the integrands $\bar{f}_j^*(r, \theta, p)e^{pt}$ in the neighborhood of $p = 0$. Using the general expression for $\bar{f}_j^*$ given by equation (20), the definitions of $\tilde{u}_{sc}^*$, $\tilde{v}_{sc}^*$ and $\tilde{\sigma}_{\theta_{sc}}^*$ given by equations (18), the small p approximations for ν_j given by equation (28), and the power series definitions of the modified Bessel functions, one finds the small p approximations to be of the form

$$\left.\begin{matrix}\bar{u}_j^*(a, \theta, p)\\ \bar{v}_j^*(a, \theta, p)\end{matrix}\right\} \sim \text{const}(\log p)^{-1}p^{-2} \tag{29a}$$

$$\left.\begin{matrix}\bar{u}_j^*(a, \theta, p)\\ \bar{v}_j^*(a, \theta, p)\end{matrix}\right\} \sim \text{const}(\log p)^{-1}p^{-1} \tag{29b}$$

$$\bar{\sigma}_{\theta_j}^*(a, \theta, p) \sim \text{const}(\log p)^{-1}p^{-2} \tag{29c}$$

where the constants are non-vanishing functions of a, c_d, c_s, and θ. The algebraic singularities of these integrand factors cause the integrals in equation (22) to diverge as δ (the radius of the indentation C_0) approaches zero; however, by using the convolution theorem, these singularities can be removed.

APPLICATION OF THE CONVOLUTION THEOREM

Because we restrict our attention to the shadow zone, where the response is identically zero for $t < 0$, the bilateral Laplace transform reduces to the one-sided Laplace transform.

The convolution theorem then has the familiar form

$$\frac{1}{2\pi i}\int_{Br_1} \bar{g}_1(p)\bar{g}_2(p)\,e^{pt}\,dp = \int_0^t g_1(\tau)g_2(t-\tau)\,d\tau. \tag{30}$$

Taking $g_1(p) = p^n\bar{f}_j^*(r, \theta, p)$ and $\bar{g}_2(p) = p^{-n}$ one obtains

$$f_j^*(r, \theta, t) = \int_0^t \frac{(t-\tau)^{n-1}}{(n-1)!}\frac{1}{2\pi i}\int_{Br_1} p^n\bar{f}_j^*(r, \theta, p)\,e^{p\tau}\,dp\,d\tau. \tag{31}$$

Again completing Br_1 by the contour C, interchanging the order of integration on p and t (justified because it was shown numerically that the $\bar{f}_j^*$ decay exponentially as $p \to \infty$ on the imaginary axis), and carrying out the integration on τ, we obtain

$$f_j^*(r, \theta, t) = -\frac{1}{2\pi i}\int_C \bar{f}_j^*(r, \theta, p)\left[e^{pt} - \sum_{k=0}^{n-1}(pt)^k(k!)^{-1}\right]dp. \tag{32}$$

Since the factor in square brackets behaves like p^n as $p \to 0$, we see from equation (29) that by using $n = 2$ for u_j^*, v_j^* and $\sigma_{\theta_j}^*$, and $n = 1$ for $\dot{u}_j^*$ and $\dot{v}_j^*$, the integrands will approach zero as $p \to 0$. Then, as $\delta \to 0$, the integrals on the indentation C_0 vanish, and we are left with

$$f_j^*(r, \theta, t) = \frac{1}{2\pi i}\lim_{R\to\infty}\int_{-iR}^{0} + \int_0^{iR} \bar{f}_j^*(r, \theta, p)\left[e^{pt} - \sum_{k=0}^{n-1}(pt)^k(k!)^{-1}\right]dp. \tag{33}$$

These integrals are proper at the origin.

NUMERICAL EVALUATION OF THE INTEGRALS

For numerical evaluation, the symmetry properties of the integrand were used to write the integral over the positive imaginary p axis, and the variable of integration was changed to the nondimensional frequency, $\Omega = \omega a/c_d$ (where $\omega = ip$). The integrand factors $\bar{f}_j^*(r, \theta, -i\omega)$ were evaluated numerically and tabulated at a fixed set of Ω values,

$$\Omega = 0{\cdot}01(0{\cdot}01)\,0{\cdot}1(0{\cdot}1)\,1(0{\cdot}2)\,40.$$

These Ω values were chosen because they were sufficiently closely spaced to make a Simpson's rule evaluation of the integral accurate to within about one percent for $0 < c_d t/a < 10$. The integral over $0 < \Omega < 0{\cdot}01$ was shown to contribute less than one percent by using asymptotic approximations, therefore its contribution was neglected. By plotting the convergence of the integrals as the upper limit was increased, it was shown that an upper limit of 40 was adequate for convergence of the velocities and displacements within about one percent except for the $P1$ mode for $\theta < \pi$ and $c_d t/a < 1{\cdot}5$, where spurious oscillations of a few percent resulted, as indicated below. For the stress σ_θ, the slow convergence of the integrals at the upper limit prevented numerical evaluation by the present techniques.

DISCUSSION OF NUMERICAL RESULTS

The displacements and velocities on the surface of the cavity ($r = a$) were evaluated at the points $\theta = \frac{3}{4}\pi$ and $\theta = \pi$ for $0 < c_d t/a < 10$. The modes $P1$, $P2$, $P3$, R, $S1$, and $S2$

were summed. Again, Poisson's ratio was taken to be $\frac{1}{4}$. The velocities have the most interesting pulse behavior and are shown in Figs. 4 through 7 for the $\theta = \frac{3}{4}\pi$ point.† We use the normalization constant $\dot{u}_0 = \sigma_0 c_d/(\lambda + 2\mu)$, which is the particle velocity behind the incident step-stress dilatation wave.

Figure 4 shows the radial velocity in the wave form of solution, i.e. $\dot{u}^*$, at $\theta = \frac{3}{4}\pi$ (both individual mode contributions and the mode sum are shown). The largest contribution comes from the $P1$ mode, which also exhibits strong impulsive behavior at the arrival time of diffracted P waves. The second largest contribution comes from the R mode. It is

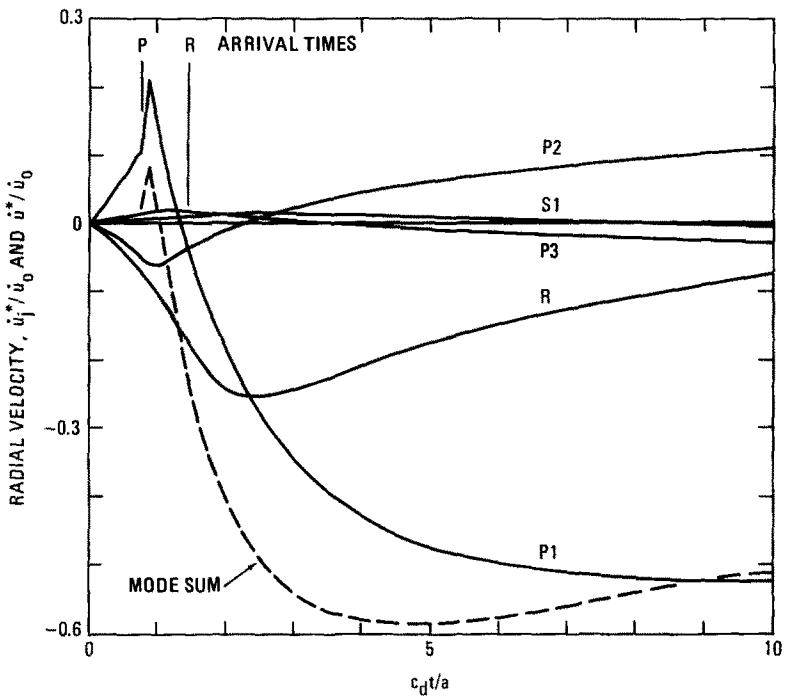

FIG. 4. Modal response $\dot{u}_j^*$ and mode sum $\dot{u}^*$ at $r = a$, $\theta = \frac{3}{4}\pi$.

noteworthy that no significant impulsive behavior occurs at the diffracted Rayleigh (R) wave arrival time. Contributions from the higher P modes ($P2$ and $P3$) are seen to decrease rapidly as the mode number is increased. The $S1$ mode has a very small contribution, and the $S2$ mode response is too small to be plotted. The mode sum is essentially zero ahead of the arrival time of the diffracted P wave. The plot in Fig. 4 is too crowded to show this, but it can be seen in Fig. 6. The slight oscillations about zero ahead of the P-wave arrival time (visible in Fig. 6) are probably caused by truncation of the infinite integrals at $\Omega = 40$, since the convergence becomes quite slow as $c_d t/a$ is decreased.

In Fig. 5, the mode contributions and mode sum are shown for the positive θ propagating $\dot{u}^*$ wave at $\theta = \frac{5}{4}\pi$. The additional propagation of $\pi/2$ in θ has effected some striking

† Results for velocities at $\theta = \pi$, and displacements at $\theta = \frac{3}{4}\pi$ and $\theta = \pi$, are presented in [20].

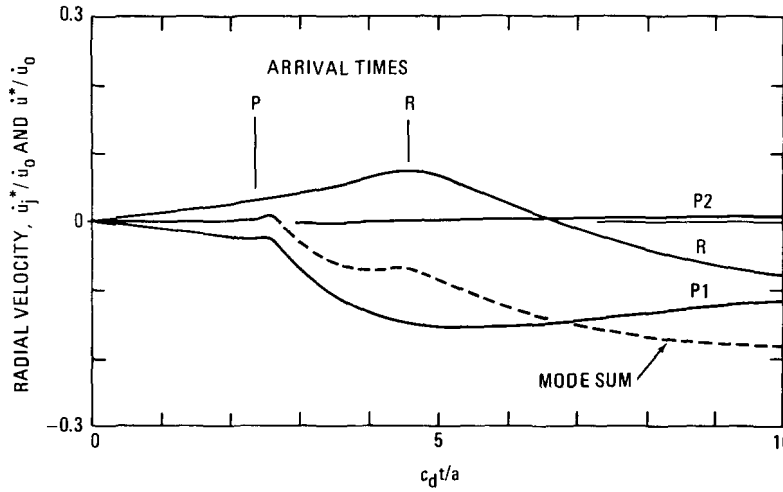

FIG. 5. Modal response $\dot{u}_j^*$ and mode sum $\dot{u}^*$ at $r = a, \theta = \frac{5}{4}\pi$.

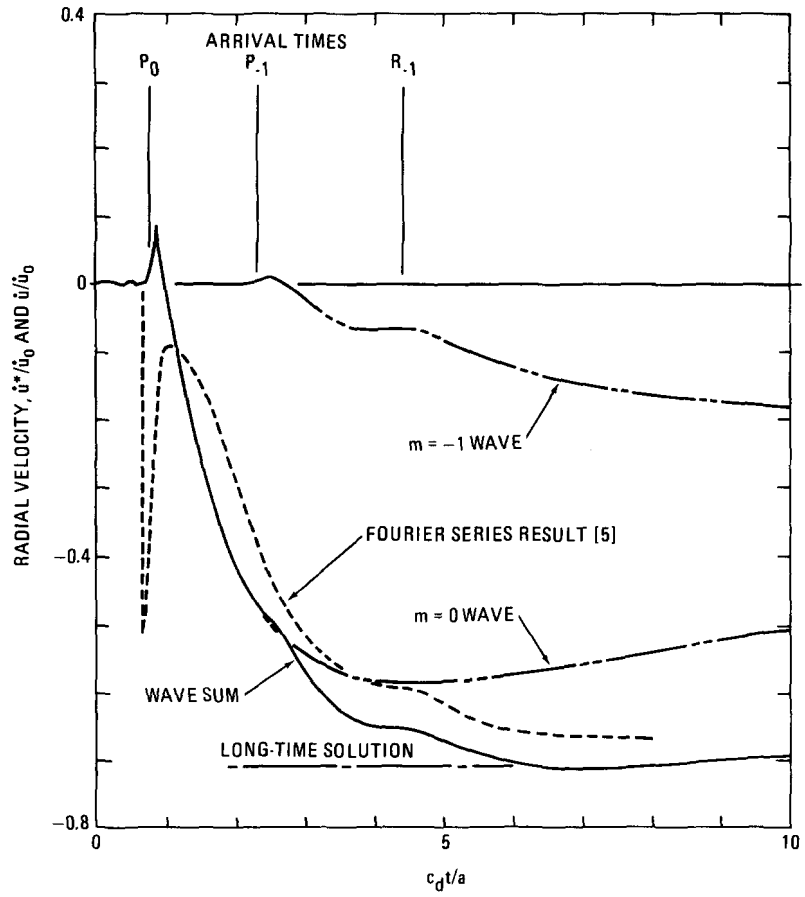

FIG. 6. Waves $\dot{u}^*$ and wave sum $\dot{u}$ at $r = a, \theta = \frac{3}{4}\pi$.

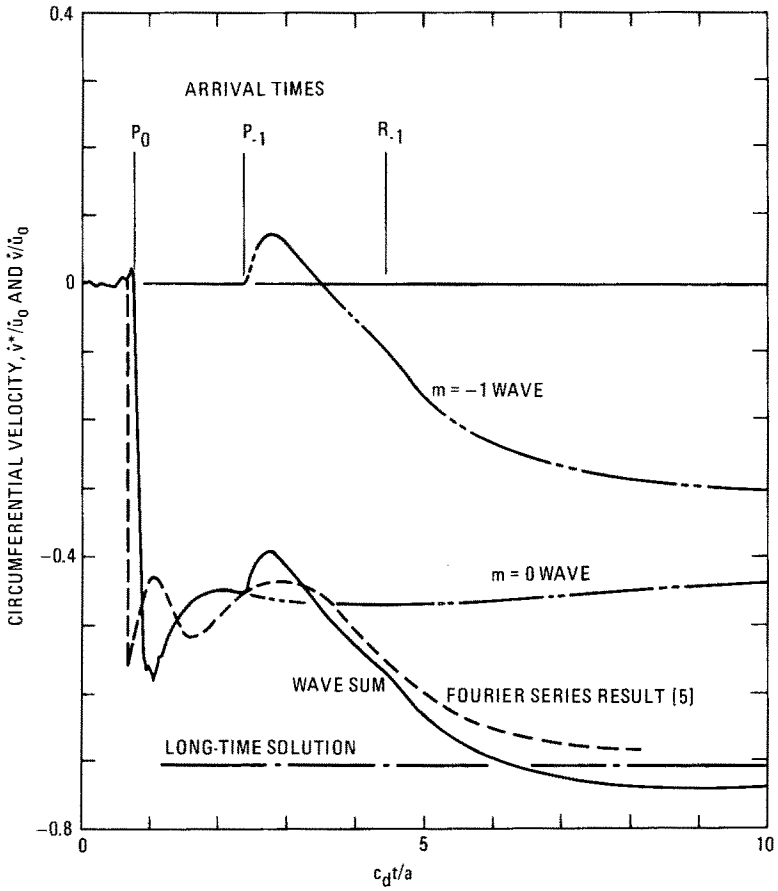

FIG. 7. Waves $\dot{v}^*$ and wave sum $\dot{v}$ at $r = a, \theta = \frac{3}{4}\pi$.

changes. The most obvious change is the decrease of amplitude of the wave. Second, the mode convergence has become even more rapid than at $\theta = \frac{3}{4}\pi$. Third, the mode sum is clearly zero ahead of the P arrival (the infinite integrals converge much more rapidly at higher θ's because of the imaginary part of ν_j) and the slow, smooth rise of the pulse from zero at the front, which is characteristic of diffracted waves (see [3]), has become apparent in the numerical results. Finally, a pulselike behavior has begun to emerge at the R wave arrival time. This delayed emergence of the Rayleigh-type pulse is similar to the behavior in the half-space problem with a buried source disturbance [23]. This behavior is also an early indication of the long-time dominance of the Rayleigh pulse predicted by Miklowitz [11].

To obtain the total response at the $\theta = \frac{3}{4}\pi$ point, the wave sum of the $\dot{u}^*$ waves must be formed per equation (6). This is illustrated in Fig. 6. The first wave to arrive is the $m = 0$ wave, which is just the $\dot{u}^*$ wave at $\theta = \frac{3}{4}\pi$ given in Fig. 4. The second wave to arrive is the $m = -1$ wave, propagating in the negative θ direction. By virtue of the symmetry of $\dot{u}^*$ in θ, this second wave is identical to the $m = 0$ wave at $\theta = \frac{5}{4}\pi$, given in Fig. 5. The $m = 1$

and $m = -2$ waves also arrive at $\theta = \frac{3}{4}\pi$ for $c_d t/a < 10$, but their contributions are negligible for $c_d t/a < 10$. Thus, the wave sum is essentially the sum of the $\dot{u}^*$ waves for $m = 0$ and $m = -1$, as shown in Fig. 6 by the solid curve. The correspondence with the long-time solution is seen to be good; the slight deviation for $c_d t/a$ approaching 10 is probably due to the neglect of the $P4$ mode in the $m = 0$ wave. The three-term Fourier results obtained by Baron and Parnes [5] are seen in fairly good correspondence except near the wave front, where the three terms are not enough to give even qualitatively correct results. The close correspondence of the present representation with the physics of the problem is exemplified by the fact that pulselike disturbances at the P_{-1} and R_{-1} arrival times are a natural part of the present representation.

The waves and wave sum for the circumferential velocity at $\theta = \frac{3}{4}\pi$ are shown in Fig. 7. Some comparisons with the radial velocity results in Fig. 6 worthy of comment are as follows: (1) a much larger disturbance is contributed by the $m = -1$ wave at the P_{-1} arrival time, which the Fourier series results tend to smooth out, (2) the Fourier series results are in better agreement near the P_0 wave front, (3) a barely detectable Rayleigh pulse occurs in the $m = -1$ wave, and (4) the short-time oscillations in the $m = 0$ wave, caused by truncation of the infinite integrals, are slightly larger than they were for the radial velocity.

CONCLUSIONS

The approach based on the wave-sum method provides better physical insight into the early-time, near-field wave motions than does the Fourier series method. The wave-sum form of solution converges rapidly at short times where the Fourier series solutions are ineffective. The convergence at long time is still fast enough so that seven modes provide an accurate solution. It must be kept in mind that, for general loading functions, the comparative convergence properties of the two methods depend on the time constants of the load. For load histories that are "more impulsive" than the step-function, the wave-sum method would be even more rapidly convergent; however, for more gradually applied loads, the Fourier series method would become more advantageous.

It is also important to recognize the disadvantages of the wave-sum method. First, numerical evaluations of the type presented, using the mode series, are restricted to the shadow zone. Second, the relatively abstruse mathematics of Bessel functions of complex order come heavily into play. Finally, the roots of a complicated transcendental equation must be evaluated before the evaluation of the inversion integrals themselves, making the overall numerics for the present approach considerably more involved than those for the Fourier series approach.

REFERENCES

[1] M. L. Baron, H. L. Bleich and P. Weidlinger, Theoretical studies on ground shock phenomena. Mitre Corporation, Bedford, Mass., Report SR-19 (October 1960).
[2] F. G. Friedlander, Diffraction of pulses by a circular cylinder. *Communs pure appl. Math.* **7**, 705–732 (1959).
[3] F. G. Friedlander, *Sound Pulses*, Chapter 6. Cambridge University Press (1958).
[4] M. L. Baron and A. T. Matthews, Diffraction of a pressure wave by a cylindrical cavity in an elastic medium. *J. appl. Mech.* **28**, 347–354 (1961).
[5] M. L. Baron and R. Parnes, Displacements and velocities produced by the diffraction of a pressure wave by a cylindrical cavity in an elastic medium. *J. appl. Mech.* **29**, 385–394 (1962).

[6] A. M. SOLDATE and J. F. HOOK, A theoretical study of structure–medium interaction. *Air Force Special Weapons Center, Report SWC TDR* 62–30 (March 1962).
[7] S. L. PAUL and A. R. ROBINSON, Interaction of plane elastic waves with a cylindrical cavity. *Air Force Weapons Laboratory, Report RTD TDR* 63–3021 (June 1963).
[8] F. GILBERT and L. KNOPOFF, Scattering of impulsive elastic waves by a circular cylinder. *J. acoust. Soc. Am.* **31**, 1169–1175 (1959).
[9] F. GILBERT, Scattering of impulsive elastic waves by a smooth convex cylinder. *J. acoust. Soc. Am.* **32**, 841–857 (1960).
[10] J. MIKLOWITZ, Scattering of transient elastic waves by a circular cylindrical cavity. *Air Force Special Weapons Center, Report SWC TDR* 63–43 (November 1963).
[11] J. MIKLOWITZ, Scattering of a plane elastic compressional pulse by a cylindrical cavity. *Proc. Eleventh Int. Congr. appl. Mech.*, Munich, Germany, 1964, 469–483. Springer (1966).
[12] C. K. GRIMES, Studies on the propagation of elastic waves in solid media. Ph.D. Thesis, California Institute of Technology (1964).
[13] F. R. NORWOOD and J. MIKLOWITZ, Diffraction of transient elastic waves by a spherical cavity. *J. appl. Mech.* **34**, 735–744 (1967).
[14] P. M. MORSE and H. FESHBACH, *Methods of Theoretical Physics*. McGraw-Hill (1953).
[15] H. M. NUSSENZVEIG, High-frequency scattering by an impenetrable sphere. *Ann. Phys.* **34**, 23–95 (1965).
[16] J. MIKLOWITZ, Plane-stress unloading waves emanating from a suddenly punched hole in a stretched elastic plate. *J. appl. Mech.* **27**, 165–171 (1960).
[17] J. R. LLOYD and J. MIKLOWITZ, On the use of double integral transforms in the study of dispersive elastic wave propagation. *Proc. Fourth U.S. natn. Congr. appl. Mech.* 255–267 (1962).
[18] I. A. VICTOROV, Rayleigh-type waves on a cylindrical surface. *Soviet Phys. Acoust.* **4**, 131–136 (1958).
[19] J. B. KELLER, S. I. RUBINOW, and M. GOLDSTEIN, Zeros of Hankel functions and poles of scattering amplitudes. *J. Math. Phys.* **4**, 829–832 (1963).
[20] J. C. PECK, Plane-strain diffraction of transient elastic waves by a circular cylindrical cavity. Ph.D. Thesis, California Institute of Technology (May 1965).
[21] M. NAGASE, On the zeros of certain transcendental functions related to the Hankel functions (parts I and II). *J. phys. Soc. Japan* **9**, 826–853 (1954).
[22] M. GOLDSTEIN, NUBES 3: Bessel functions for complex argument and order. SHARE Program 979 (October 5 1960).
[23] W. M. EWING, W. S. JARDETZKY, and F. PRESS, *Elastic Waves in Layered Media*. McGraw-Hill (1957).

(*Received* 13 *May* 1968; *revised* 21 *October* 1968)

Абстракт—Настоящая работа исследует двухмерное взаимодействие волны сжатия типа ступенчатой функции в бесконечно упругой среде с круглой полостью. Представленный здесь способ расчета является применением метода разработанного Фридляндером для приближений фронтов волн. Метод фридляндера оказывается более эффективным для коротких интервалов времени по сравнению с решением в рядах Фурье. В представленной работе применяется, впервые, численный анализ к методу Фридляндера. Этот анализ пригоден только в районе отражения полости, так как только в этом районе можно построить решение для переходных характеристик в рядах для круглых форм распространения. Эти формы определяют диспершрующий спектр при отношении комплексных чисел волн к частоте. Представляются численные результаты для семи форм спектра. Полученные формы используются для построения поперечных скоростей на задних поверхностях полости. Численные результаты указывают на очень быструю сходимость рядов для форм, при коротких интервалах времени, а также, что семь форм оказываются достаточными для определения асимптотических значений для длинных интервалов времени. По сравнению с предыдущими результатами в рядах Фурье, настоящее решение не содержит неточности в некоторой степени, при коротких интервалах времени, которая существует для решения в рядах.